Nuclear Materials and Energy 19 (2019) 503–509

Contents lists available at ScienceDirect

Nuclear Materials and Energy

journal homepage: www.elsevier.com/locate/nme

# Laser-Induced Desorption of co-deposited Deuterium in Beryllium Layers on Tungsten

M. Zlobinski[a,*], G. Sergienko[a], Y. Martynova[a], D. Matveev[a], B. Unterberg[a], S. Brezinsek[a], B. Spilker[a], D. Nicolai[a], M. Rasinski[a], S. Möller[a], Ch. Linsmeier[a], C.P. Lungu[b], C. Porosnicu[b], P. Dinca[b], G. De Temmerman[c]

[a] Institute of Energy and Climate Research – Plasma Physics, Forschungszentrum Jülich GmbH (FZJ), Partner in the Trilateral Euregio Cluster, D-52425 Jülich, Germany
[b] National Institute for Laser, Plasma and Radiation Physics (INFLPR), Atomistilor 409, Magurele, Jud Ilfov, 077125 Bucharest, Romania
[c] ITER Organization, Route de Vinon-sur-Verdon, CS 90 046, 13067 St Paul Lez Durance Cedex, France

ARTICLE INFO

*Keywords:*
Fuel retention
Beryllium
Tritium monitoring
Laser
Desorption
FREDIS

ABSTRACT

For the development of the tritium monitoring system in ITER the hydrogen isotope release by Laser-Induced Desorption (LID) from Be layers is studied to determine the laser parameters for a high desorption efficiency while minimising dust production and surface modifications is also pursued. Be layers of 1 μm thickness with 25–30 at% D and $3 \times 10^{22}$ D/m$^2$ comparable to JET-ILW areal concentrations [1] have been produced by High Power Impulse Magnetron Sputtering (HiPIMS) on ITER grade W. Laser pulses of 1, 5 and 10 ms duration heat the layer in vacuum in the Fuel REtention DIagnostic Setup (FREDIS) and release the retained D thermally. By mass spectrometry in FREDIS and subsequent Nuclear Reaction Analysis (NRA) inside the laser spot the desorbed and remaining D is quantified. While a pulse duration of 1 ms cannot fully desorb the deuterium, it is found that a single 5 or 10 ms laser pulse with an absorbed energy density of ca. 1.5 MJ/m$^2$ corresponding to a heat flux factor around 20 MW√s/m$^2$ leads to nearly complete desorption of the retained D. This encourages the development of a useful tritium monitoring system, although the present layers produce some dust due to local delamination of the layer on at least 11% of the heated surface (at 1.4 MJ/m$^2$ absorbed energy within 5 ms) and lead to unavoidable crack formation.

## 1. Introduction and motivation

In fusion devices with beryllium (Be) and tungsten (W) as plasma-facing materials such as the JET-ILW, the major contribution to the long-term hydrogen retention is found in co-deposited Be layers on W divertor components [1]. In ITER, the formation of hydrogen isotope containing Be layers is expected, which may occur on different wall elements, mainly on the divertor baffles [2]. These layers will contain also tritium (T), but the tritium retention is limited by the nuclear license. To study and monitor the spatial distribution of the H, D and T content of the wall without tile removal, a pulsed Laser-Induced Desorption (LID) system is being designed as fuel retention diagnostic detecting released hydrogen isotopes between plasma pulses by means of mass spectrometry [3]. Apart from this, LID could even be used during plasma operation detecting the desorbed gases spectroscopically [4].

According to numerical desorption calculations for Be [3] optimised laser pulse parameters (laser intensity, pulse duration etc.) should yield a high desorption fraction. An experimental verification is provided in the present work, whereby the influence of different laser pulse parameters on the desorption efficiency of LID is studied on Be layers. The objective of the present study is to validate experimentally the use of long laser pulses on beryllium co-deposits for tritium retention measurement purposes.

## 2. Samples

The tritium monitor system in ITER is designed to probe an area in the divertor region. In order to resemble as close as possible the expected ITER wall in that position, W substrates of the ITER grade were chosen, which were produced by Plansee SE [5] and have a grain elongation perpendicular to the surface. Two types of samples were cut: small samples of 5 mm × 5 mm × 5 mm and large samples of 36 mm × 36 mm × 5 mm and one surface was polished. Be test coatings on 4 differently rough surfaces were done to find a trade-off between good layer adhesion and a flat surface for good surface analysis resulting in a polishing with a finish of 1 μm diamond grains. The

* Corresponding author.
*E-mail address:* m.zlobinski@fz-juelich.de (M. Zlobinski).

https://doi.org/10.1016/j.nme.2019.04.007
Received 14 August 2018; Received in revised form 26 February 2019; Accepted 4 April 2019
Available online 14 April 2019

**Table 1**
Be layer composition of a 1 μm thick HiPIMS layer with D co-deposition, before laser heating, according to NRA (for D content), LID-QMS (for H content) and EDX.

| Sample size: Element | Small at% | Large at% |
|---|---|---|
| Be | 70–72 | 67–69 |
| D | 25–27 | 28–30 |
| H | 1.1 | 1.1 |
| O | 1.0 | 1.9 |
| C | 1.8 | 0.6 |
| N | 0.4 | 0.4 |

arithmetic mean roughness on the length scale of 1 mm showed values of ca. 10 nm for the small samples and 20 nm for the large sample. The W samples were coated with a 1 μm thick Be layer, that was produced by High Power Impulse Magnetron Sputtering (HiPIMS) in INFLPR, Bucharest [6]. The base pressure in the vacuum chamber was $3 \times 10^{-4}$ Pa and increased to 2 Pa after the inlet of the processing gases Ar and $D_2$, which was used during the sputtering process to co-deposit D in the layer. NRA measurements [7] show a D concentration of 25–30 at%. Combined with EDX (Energy-Dispersive X-ray spectroscopy) measurements of the unheated layer the following layer composition was determined (cf. Table 1).

This variation of the D content was observed on samples that were coated simultaneously in a single coating run. However, for the small samples the resulting D areal concentration is very similar with $(3.01–3.07) \times 10^{22}$ D/m$^2$ despite the slightly different relative D fraction. Within the large sample the values vary stronger: $(2.4–3.6) \times 10^{22}$ D/m$^2$, (cf. Fig. 8b and its discussion) while the Be/D ratio is nearly constant. Thus the layer inhomogeneity is due to changes in layer thickness. It should be noted that these areal concentrations are similar to those found on tokamak divertor tiles [1].

The pulsed deposition process in HiPIMS continued without interruption for 57 h at a sample temperature of ca. 340 K with unchanged power of several MW/m$^2$ applied during 3 μs long magnetron pulses. The layer thickness of 1 μm was verified by SEM (Scanning Electron Microscopy) on the cross section of a Si witness sample exposed simultaneously.

## 3. Experimental and evaluation methods

LID is performed in FREDIS [8] in the High temperature Materials Laboratory (HML) in Jülich where Be samples can be handled due to a closed glove box system attached to the vacuum chamber. The sample is located on a copper block below the anti-reflexion (AR) coated window, while the laser light is guided through a fibre-optic cable to the laser head, which images the circular end of the fibre by two lenses sharply onto a 3 mm diameter spot on the sample. A two-colour pyrometer observes the inner part of the laser spot via a second fibre through a beam splitter vertically from the top. Before the laser pulse, the shutter to the turbo pump is closed at about $10^{-5}$ Pa base pressure and the Quadrupole Mass Spectrometers (QMS) measure the continuous partial pressure increases from metal outgassing and leaks. Then the laser pulse heats the surface rapidly, the retained gases are released thermally and desorb promptly giving a sharp jump in the corresponding partial pressures, here mainly HD (m/$q$ = 3 amu/e) and $D_2$ (m/$q$ = 4 amu/e). Afterwards, the shutter to the pumping system is opened again. The evaluation of the QMS signals is based on the maximum peak values, that are fitted by an exponential function before and after the laser pulse (cf. Fig. 1). Both functions are extrapolated to the time of the laser pulse, where the jump in each mass channel is evaluated as difference between the two functions. This difference is converted to the amount of released D atoms based on QMS calibration during constant inlet of $H_2$, $D_2$ and other gases from calibration leak standards with fixed gas

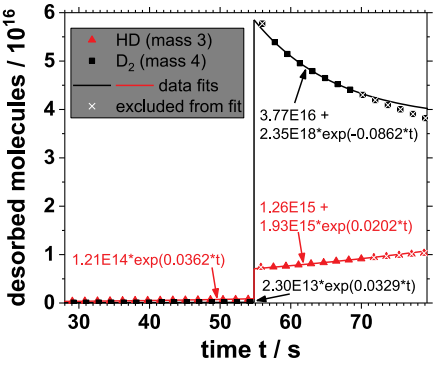


**Fig. 1.** Temporal behaviour and corresponding fits of the QMS data before and after LID with 2.1 MJ/m$^2$ absorbed energy within 10 ms. For these samples 90–96% of the desorbed D is detected on mass 4.

reservoir (provided by LACO). While the leak is open, the shutter to the pumps is closed like in the LID experiment, resulting in an almost linear increase of the partial pressure of the calibration gas and the QMS peak of the corresponding mass with a slope in units of A/s. The ratio of this slope and the amount of molecules per second of the calibration leak entering the chamber yields the calibration factor in molecules/A for each gas. The calibration factor for HD is deduced as the average of the calibration factors for $H_2$ and $D_2$.

The laser pulse shape is shown in Fig. 2 for the three pulse durations. While it is nearly rectangular for the 1 ms pulse, the laser power considerably decreases continuously during the laser pulse for longer laser pulses. Thus, the results will be presented as a function of laser energy density rather than power density, which is not constant during the pulse for the non-rectangular pulse shapes. This value is thus better comparable to other laser systems.

After LID the samples were transferred to the NRA chamber where the NRA beam of $^3He^{++}$ was magnetically compressed in size to ca. 1 mm (0.84 mm × 0.68 mm) to fit into the centre of the laser spots. The positioning has been done on a scintillator plate where the beam size, shape and position could be seen directly. The beam energy of 4.5 MeV was more than sufficient to easily penetrate the 1 μm Be layer as it would reach more than 20 μm deep in pure Be and even reaches ca. 7 μm deep into the W substrate. Only the measurements on the small sample before laser heating were done at 2.95 MeV, which is still sufficient for a thickness of 1 μm Be as a depth of 13 μm could be reached in pure Be and about 4 μm deep into the W substrate. Hence, all D in the layer and these ranges was detected by measuring the proton (p) from the reaction D($^3$He, p)$^4$He. For the quantification of Be the proton from the reaction $^9$Be($^3$He, p)$^{11}$B was used. The D and Be amount were quantified by simulating the measured spectra by the programme SIMNRA [9] and changing the D and Be amount until the D and Be integrals of the measured and simulated spectra were identical between simulation and model. For the simulation a model system of a quasi infinite W substrate was used with a layer of variable amount of atoms consisting of Be and D. For the low D concentrations inside the laser spots with high desorption the D values are rather overestimated as the

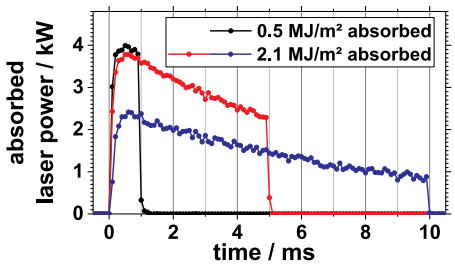


**Fig. 2.** Applied laser pulse shapes.

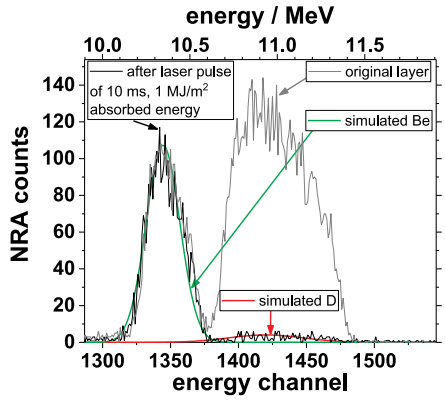


**Fig. 3.** NRA data of the unheated layer and inside a laser spot and simulated Be and D peaks.

border of the D peak is not clearly recognisable in the measured data. Therefore, the integration is extended to high-energy regions where the simulated D peak has practically decreased to 0 already, but still some scattered NRA signal counts were measured there (cf. Fig. 3). They are thus probably originating not from D but some impurities like N, O etc. Taking them into account in the integration of the D peak leads to an overestimation of the D content, which is increasing the relative error with decreasing D amount.

The surface of the laser spots was also analysed by SEM imaging before NRA in detail for the effects of delamination, melting, cracking and also at low magnification to obtain overview images of the most interesting laser spots (Fig. 4a). These were analysed to determine the delaminated area by applying a graphical method based on image brightness. As confirmed by EDX on the differently bright regions, the dark grey areas are nearly pure Be and thus represent the areas with best attachment and probably original thickness (cf. Fig. 4c). The white areas correspond to the W substrate, while the brighter grey areas seem to represent a thin Be layer at the interface to the W that is still well attached to the substrate. The shadows which are strong around the thick dark Be layer, but not visible at the edges of the thin Be layer indicate that the thick Be layer is probably not firmly attached. Due to its small thickness the thin layer is not assumed to contain significant D amounts. Thus, in the graphical method the white areas of the substrate and the bright grey areas of the thin layer are both treated as delaminated areas. They are marked as black pixels (cf. Fig. 4b) by means of threshold contrast, i.e. defining a grey level threshold below which a pixel is set to black and above to white. The area outside the laser spot was excluded from the analysis by a circular mask of 3 mm in diameter. All black pixels are summed and converted by the scale factor of 6.4 $\mu m^2$/pixel into a delaminated area. The result can be seen in Table 2

**Table 2**
Estimation of the missing Be amount in the LID spots depending on the laser pulse length $t_p$ and absorbed energy density ε by four methods (cf. text for details), *italic* data are from the small sample; missing data are due to spots for which no analysis was performed.

| $t_p$ | $\varepsilon_{absorbed}$ | SEM Full spot | SEM Inside | RBS | NRA |
|---|---|---|---|---|---|
| ms | $MJ/m^2$ | % | % | % | % |
| 1 | 0.2 | | | 11 | 11 |
| 1 | 0.2 | 4 | 9 | 19 | 25 |
| 1 | 0.5 | | | 89 | 93 |
| 1 | 1.4 | 103 | 97 | | |
| 5 | 0.5 | 0.4 | 4 | | |
| 5 | 0.6 | 0.3 | 1 | 3 | 11 |
| 5 | 1.4 | 66 | 86 | 87 | 85 |
| *5* | *1.4* | *11* | *15* | *25* | *−4* |
| 5 | 2.1 | 63 | 60 | 64 | 39 |
| 10 | 0.8 | 0 | 0 | 1 | 12 |
| 10 | 0.9 | 1 | 5 | 8 | 26 |
| 10 | 1.0 | 31 | 82 | 77 | 76 |
| 10 | 1.0 | 0.05 | 0.2 | 3 | 20 |
| 10 | 2.1 | 13 | 25 | 36 | 36 |

row “SEM Full spot”. The same analysis was performed also inside the laser spots, where it was restricted to the region, which was analysed by the NRA beam (cf. “SEM Inside” in Table 2).

For the NRA analysis, the amount of missing Be is important as it is performed after LID and thus cannot detect the undesorbed D in the delaminated fragments that are missing from the surface. Moreover, the transfer of the sample to the NRA chamber probably increased the amount of delaminated Be as after unmounting in FREDIS, the samples had to be blown off with air in the glove box for Be safety in order to minimise Be dust that could contaminate the SEM and NRA chambers.

The column “NRA” in Table 2 gives an estimate of the missing Be based on the reduction of the NRA signal for Be (cf. left peak in Fig. 3) inside the LID spot with respect to the original layer. A fourth estimation method was used based on the RBS signal (cf. column “RBS” in Table 2), which utilises the reflexion of the impinging He particles on the sample. In the delaminated areas they are reflected on the W substrate and thus reach the RBS detector with a higher energy than those reflected on the Be layer. Hence, two reflexion edges can be identified in the RBS spectrum and their relative height is used here as an estimation of the delaminated area.

## 4. Results and discussion

The results are presented in terms of the absorbed laser energy or heat flux factor, for better comparability to other heating systems. However, the absorbed values have some uncertainties due to the

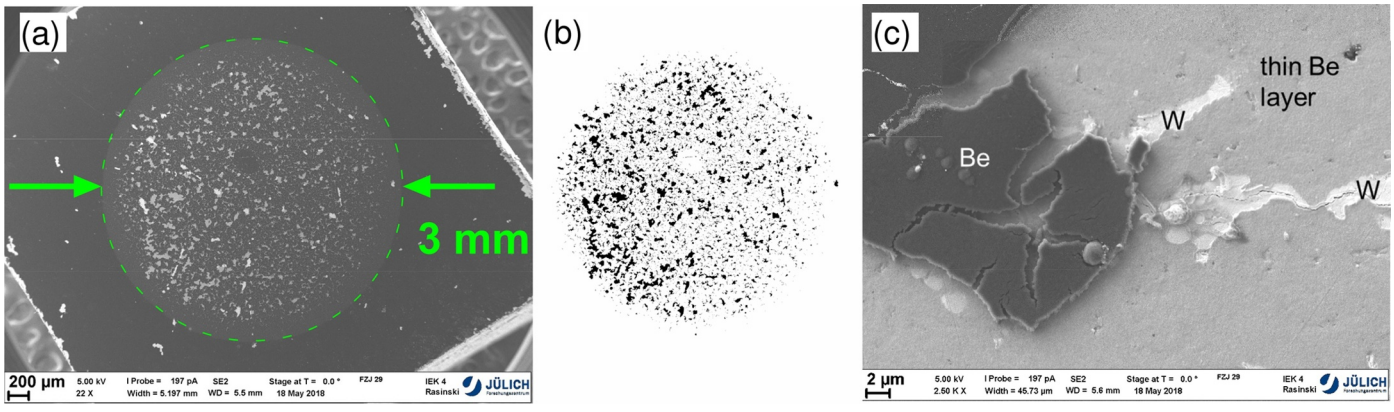


**Fig. 4.** SEM analysis of the small sample illustrates layer delamination after one LID pulse (10 ms, 1.4 $MJ/m^2$ absorbed): (a) full spot, (b) graphical determination of delaminated area, (c) thin Be layer remains attached to W.

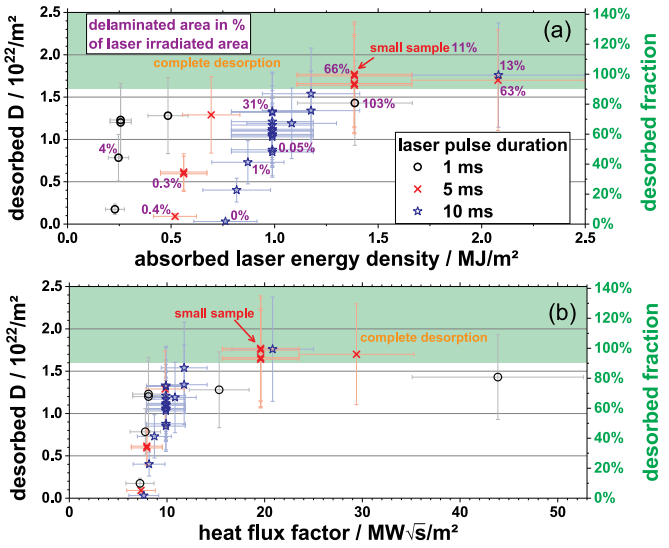


**Fig. 5.** Desorbed D during LID as measured by Quadrupole Mass Spectrometry; (a) as function of laser energy density, (b) as function of the heat flux factor.

energy losses on the light path from the laser to the target and due to the reflexion on the sample. The losses on the light path were estimated by measuring the laser energy at the laser exit before it is coupled by a lens into the fibre-optic cable and after the laser head, just before the anti-reflexion coated vacuum window. Losses of ca. 20% were measured. The reflexion of the laser light on the sample was measured with a spectrophotometer in the UV, VIS and IR range and the value at the laser wavelength of 1064 nm of 38% total reflectivity was used for calculation of the laser energy which is absorbed by the sample and transformed into heat. As the reflectivity is measured only at room temperature, there is quite high uncertainty how it develops during the laser heating. Thus the absorbed laser energy and heat flux factor are shown with a relative error of ± 20%.

The QMS results of the desorbed D during LID in Fig. 5a show a sharp threshold for desorption at ca. 0.25 MJ/m$^2$ for 1 ms laser pulse duration, 0.5 MJ/m$^2$ for 5 ms pulse duration and 0.75 MJ/m$^2$ for 10 ms pulse duration. The energy variations at the onset of desorption were performed with very small energy steps to investigate these threshold regions carefully. It must be noted, that no desorption can be observed below the corresponding threshold – thus the term threshold is justified. The slope of the increase in desorption is larger the shorter the pulse duration. This is attributed to the temperature gradient at the laser spot edge during heating, which is larger for short laser pulses as the lateral heat diffusion is less important on short timescales. For the long laser pulses the gradient is smaller and thus the central area of maximum temperature is smaller in relation to the irradiated area for the same maximum temperature. With higher laser energy this hot central area increases for long pulses, which leads to gradually higher desorption, while for short pulses it is roughly equal to the irradiated area already for lower energies. The multitude of 10 ms data at 1 MJ/m$^2$ is due to a vertical and horizontal line scan along the edges of the large sample that was performed with identical laser pulse parameters to estimate the homogeneity of the D content in the layer (cf. discussion below). The spread of these data points has to be assumed as uncertainty or variation due to spatial inhomogeneity of the D content and can be applied to all data points. For high energies all pulse lengths seem to saturate at a given maximal desorption capability. For the 5 ms and 10 ms pulses this value is identical indicating that they fully desorbed the laser spot, while for the 1 ms a maximum of 80% of this value could be observed. The reason is probably an effect of D diffusion in the Be layer, which could be too slow to achieve a diffusion length that is larger than the layer thickness and thus the D might not be able to reach the surface. A different interpretation can be drawn from the percentage values next to the data points. They show the ratio of delaminated area to the laser irradiated area (as obtained graphically from SEM images, cf. Section 3). The highest data point for the 1 ms pulse duration is nearly fully delaminated. In its interior still some spots with Be layer are remaining, which leads to a value of 97% in Table 2, but additionally some areas just outside the irradiated area were delaminated, which gives a delamination of 103% for the full spot relative to the irradiated area. Thus, it could be speculated that in such a strong case of delamination some detached Be fragments might not be heated sufficiently for complete desorption before detachment. However, for the QMS detection during LID this is rather unlikely as the formation of cracks is assumed to occur in the cooling phase (see discussion of surface modifications below). This process is probably a precursor to the local delamination of small fragments of the layer. Thus, the heating of these fragments should already have passed the temperature maximum. Additionally, if layer fragments detach during the cooling phase they will have strongly reduced heat contact to the material below and around them, which would retard the cooling and thus increase the duration of the hot phase. All these effects should only lead to increased hydrogen isotope diffusion inside the material and increased desorption. In conclusion, the D release during LID can only be larger than the D amount that would desorb from a firmly attached layer.

Concerning the delamination data in Fig. 5a (cf. Table 2 column "SEM Full spot"), it can be stated that rather significant desorption of about half of the D inventory is possible with delamination around or less than 1%. This means that dust production can be kept small at least for moderate desorption fractions. However, comparing these low values in Table 2 to the corresponding values of missing Be obtained by RBS or NRA, higher values are found. These are most probably not due to evaporation of Be that would lead to a thinner layer because in the SEM analysis no signs of evaporation like porous structures on detached parts could be found that are typically prone to overheating. The reason is rather layer detachment of less than 1 µm thickness, which was observed in some SEM images and proven by decreased Be amount detected by EDX. These areas have still the same brightness as the thick Be layer and thus are not detected by the graphical method, while the Be amount is locally reduced.

In Fig. 5b the same QMS data are plotted against the heat flux factor (HFF), which is the laser intensity times the square root of the pulse duration. This quantity is proportional to the temperature increase by a square heat pulse in a simple one dimensional heat diffusion model and can thus be seen as a measure for the temperature that a perfectly attached homogeneous layer would reach. Although this is not the case for our layers, the HFF can still be used as an approximate measure of the temperature increase as the data fall to roughly one broad curve. It shows a common desorption threshold of ca. 7 MW√s/m$^2$ and almost complete desorption is achieved around 15–20 MW√s/m$^2$ for the longer pulse durations. Due to partial delamination of the layer, the pyrometer measurements show jumps and additionally differently varying emissivities at different wavelengths. Thus, they are not very reliable and

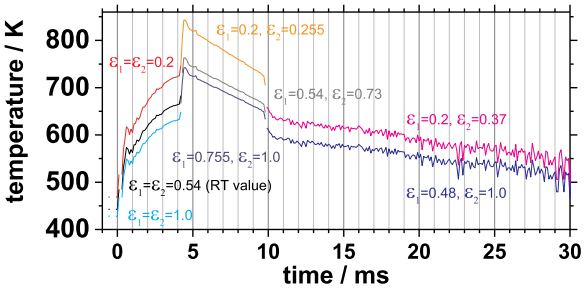


**Fig. 6.** Example of pyrometer signal during an LID pulse of 10 ms with 0.87 MJ/m$^2$ abs. energy density with different assumptions of emissivities $\varepsilon 1$ and $\varepsilon 2$ at the two detector wavelengths (1.66 µm and 1.8 µm); emissivity at room temperature (RT) was measured to $\varepsilon 1 = \varepsilon 2 = 0.54$.

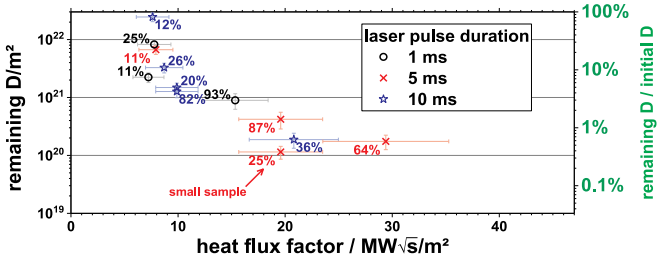


**Fig. 7.** D remaining in the laser spot after a single LID pulse as measured by NRA; the values in the graph indicate the individual increase of the data points according to the missing Be (cf. Table 2).

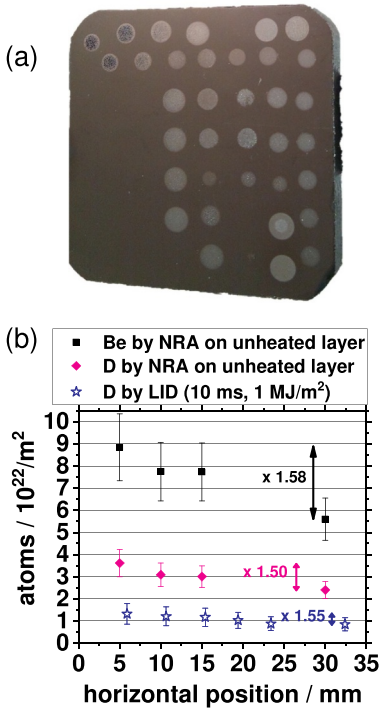


**Fig. 8.** Be layer homogeneity in Be and D content.

difficult to interpret (cf. Fig. 6). However, under the assumption of a perfectly adhesive Be layer, heat calculations lead to an expected surface temperature of roughly 650 K for 7 MW√s/m$^2$ and around 1300–1400 K for 18 MW√s/m$^2$, which is necessary for almost complete desorption. The beginning of the marked area of "complete desorption" is placed 10% below the maximum QMS values, which are about a factor of 1.3 below the lowest NRA data for the original D content (cf. Fig. 8b). The error bars of the highest QMS and lowest NRA data overlap, but the agreement is not satisfactory. Nevertheless, several facts show that the QMS data in the marked region represent full desorption. On the one hand, the maximum values have been reproduced several times with different laser parameters without showing a large scatter, which is characteristic for a hard desorption limit. On the other hand, the remaining D content was measured by NRA after desorption (cf. Fig. 7) showing 1% or less D remaining in the centre of some laser spots. Thus, the difference of the maximum QMS and NRA data is probably due to a calibration issue of the QMS as it shows some saturation effects or evaluation of NRA which is performed with nuclear cross-sections obtained at different angles than used in the measurement setup. However, the NRA signal of the unheated Be layer is two orders of magnitude larger than in the laser heated spots. As the initial D content of the layer is spatially inhomogeneous (see discussion below and Fig. 8b) an average value was used for the right scale of Fig. 7. The measured NRA data are lower than shown in the figure as they were scaled up by a correction factor for the missing Be. As the maximum correction factor is given by different methods for different laser spots, the highest correction value was chosen for each spot (i.e. in each line of Table 2) in order not to underestimate the remaining D by the choice of a single compensation method. The chosen correction value labels the data points in Fig. 7.

The NRA results show in general a decreasing amount of remaining D with higher heat flux factor – as expected. At a HFF of about 10 MW√s/m$^2$ the remaining fraction drops below 10% of the initial inventory. Above ca. 20 MW√s/m$^2$ even less than 1% of the initial D is remaining, which virtually is complete desorption of the D from the layer. The four correction methods for the NRA results were presented in Section 3. Their results (cf. Table 2) show that the delaminated amount not only depends on the laser parameters but also on the position on the sample as spots with identical laser parameters show very different extents of delamination. Comparing the 10 ms pulses with 1.0 MJ/m$^2$, the first spot was located a few mm from the left edge of the sample, where the adhesion of the layer was decreasing and the D and Be content are higher (cf. Fig. 8). The second spot was on the right hand side (horizontal position: 23 mm) in a large area of relatively good adhesion. Thus, all compensation methods show strongly reduced delamination. A similar effect is seen for the 5 ms pulses with 1.4 MJ/m$^2$, where the first spot is located on the large sample, while the second one (italic text) is on the small sample. It was in general observed that the layer adhesion is better on small samples probably due to easier stress release. The negative value for the small sample using the NRA method can probably be explained by the reference Be value used for the undesorbed case, which was taken from a previous NRA measurement on this sample at lower beam energy (cf. Section 3). All other values are referred to the average value of Be content on the large sample and are measured with the same NRA settings and on the same day as the laser spots.

For all results concerning D and Be content presented here an additional error margin has to be kept in mind due to the inhomogeneity of the layer on the large sample and differences between the layer properties on the small and large sample. In horizontal direction the layer shows the highest inhomogeneity which is observed by different methods (Fig. 8b). The Be and D contents measured by NRA in four unheated positions on the large sample show gradients towards the left side (small horizontal value) with a factor of 1.5–1.6 between the outermost positions. The same gradient is seen in a horizontal line scan by LID at constant laser parameters (10 ms, 1 MJ/m$^2$ absorbed energy density) at the top of the sample (2nd row from top in Fig. 8a). Already by visual inspection a different modification of the surface can be seen for the last two spots on the left, where the D and Be concentrations are highest. Here, the pyrometer signals were also much higher compared to the other spots of the line scan. A vertical LID scan (last column in Fig. 8a) with the same laser parameters along the right edge of the sample also shows a gradient in D content but with a smaller span of factor 1.3. As the homogeneity of the sample is better in the vertical direction and the layer shows quite different surface behaviour on the left quarter compared to the rest of the sample, the most homogeneous rectangular area on the centre and right hand side were chosen for most LID studies. Here, the variation of the D content is limited to a factor of 1.07 in vertical and 1.37 in horizontal direction (with respect to Fig. 8).

As the surface modifications like delamination play a role in the interpretation of the desorption results, two figures with the most characteristic effect are shown. In Fig. 9 the evolution of cracking and delamination is shown as suggested by the SEM observations. Except in the edge region of the laser spots, a high density of Be hills is always found (Fig. 9a). The hills seem to be the beginning of the destruction process. We assume that they are formed during the heating phase due to the higher linear expansion coefficient of Be compared to W. Thus, even if the layer and substrate temperatures are equal the Be expands more and the excess material forms these hills probably at weak points of the layer, i.e. where the internal layer stiffness or adhesion to the

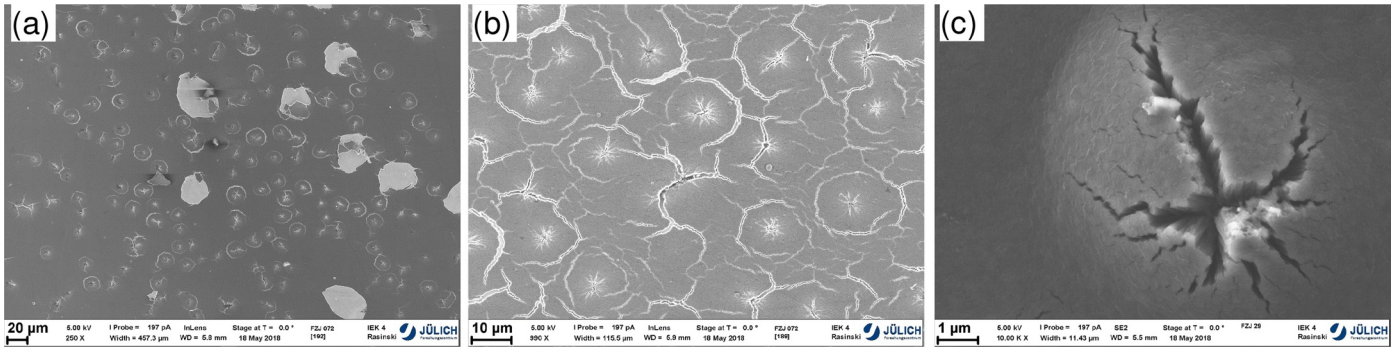


**Fig. 9.** Surface modifications due to one laser heating pulse of 5 ms duration; SEM images; (a) individual circular cracks around Be hills (0.52 MJ/m$^2$ absorbed); (b) crack network formation (0.56 MJ/m$^2$ absorbed); (c) magnification of a Be hill on the small sample (1.4 MJ/m$^2$ absorbed).

substrate is low. In the pyrometer evolution curves (cf. Fig. 6) a sudden jump is seen, which might be attributed to the hill formation as the continued laser irradiation probably heats these hills to higher temperatures than the attached regions. This is assumed because the heat contact of the hills is probably lowered. A zoom on a typical hill (Fig. 9c) shows that they are always cracked radially while the substrate cannot be seen in the cracks. Even at high laser energies as in this example no sign of evaporation or melting can be seen on the top of the hills as the crack edges are sharp and no porous areas are observed. Around almost each Be hill a large circular crack is seen, which is probably appearing during the cooling phase due to the material contraction. A thermo-mechanical force seems to act radially towards the hill centre. For cases with stronger cracking a whole crack network can be formed (Fig. 9b) which consists of the previously described large circular cracks and additionally smaller cracks that interconnect those. Delamination is probably a consequence of the cracking process as the detached areas are about 10–20 µm in size and quite circular in shape (Fig. 9a). This would indicate that such a fragment can detach, when the cracks enclose an area completely. Due to the inhomogeneous surface morphology with cracks, hills and detached parts, the pyrometer measurements cannot provide a sensible surface temperature, but at best a value dominated by the hot spots. Additionally, the data suggest strongly varying Be emissivity and changing ratios of emissivities at different wavelengths, that need further investigation.

Some high magnification images (Fig. 10) show the layer microstructure before and after laser pulses with increasing heat flux factor. The original structure is “cloud-like” (Fig. 10a), which is a characteristic of the high D fraction. The microstructure is similar to those observed on Be layers formed in JET-ILW except that there is no predominant growth direction due to magnetic field orientation in our layers. After a weak laser pulse not far above the desorption threshold (Fig. 10b) no significant modifications are visible. For stronger heating in the complete desorption regime the general microstructure is preserved but the edges of the cloud-like structures are sharper (Fig. 10c). Only for very high HFF (Fig. 10d), where melting of Be occurred, the microstructure strongly changed to a dendritic form, which is characteristic of Be oxide formation [10], which appears in brighter grey, while the dark areas are still pure Be.

In the literature, complete D desorption has only been observed at the Be melting temperature utilizing 25 ns laser pulses [11]. Only 20–60% of the retained D could be desorbed without melting. The use of laser pulses in the nanosecond range is often attributed to local melting and ablation by the laser. For controlled heating, millisecond pulses are much more suitable. However, also previous experiments in the millisecond range could only release a small fraction of up to 25% of the retained D utilizing a 10 ms pulse duration with 2 MJ/m$^2$ absorbed energy density [12]. This experiment was performed at PISCES-B on three differently produced Be layers: collection plate next to the plasma, Be evaporation into the plasma and magnetron sputtering outside PISCES, which are probably most similar to our layers. The collection plate layers showed no delamination even after the laser pulse [13], contrary to our layers. Hence, one reason for the huge difference in desorption efficiency to our experiments could be a difference in layer characteristics, especially in layer strength and adhesion to the W substrate. This is also supported by the temperature evolutions in the pyrometer measurements. While fast jumps occur during LID in FREDIS, which are attributed to the formation of the Be hills, during heating at PISCES such temperature jumps were not observed [13]. This indicates that no Be hills were formed there, which was confirmed by surface analysis, resulting in better thermal conductivity of the layer to the substrate and possibly lower maximum temperature reached in the layer. Another reason for the discrepancy might be the sample, layer and spot geometry. While for the FREDIS experiments the whole sample surface was coated and circular parts of it were heated by the laser, in PISCES only circular or elliptical parts of the sample surface were coated and the laser spot size and shape were adjusted to their geometry. Hence, there might be some effects at the edges of the layers due to the masks used during layer production or due to the oblique incidence of the laser creating an elliptical spot.

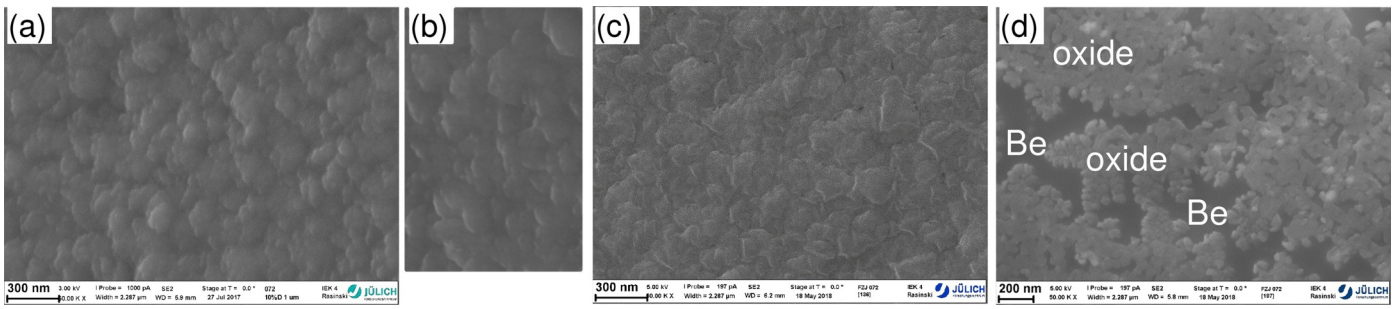


**Fig. 10.** Modifications in microstructure of the Be layer due to laser heating, SEM images all in identical magnification; values are estimated absorbed quantities; (a) before laser pulse; (b) after 1 laser pulse of 1 ms (0.25 MJ/m$^2$ absorbed, 7.8 MW√s/m$^2$); (c) after 1 laser pulse of 10 ms (2.1 MJ/m$^2$, 21 MW√s/m$^2$); (d) after 2 laser pulses (10 ms, 0.8 MJ/m$^2$, 8 MW√s/m$^2$ and 1 ms, 1.4 MJ/m$^2$, 44 MW√s/m$^2$).

## 5. Summary

Despite some layer inhomogeneities within a factor of 1.6 in D and Be content on the large sample, fairly uniform layers of ca. 1 µm thickness with a quite similar D fraction of 25–30 at% were desorbed thermally by LID. While short laser pulses with a duration of 1 ms could not fully desorb the D in the layer up to a HFF of roughly 44 MW√s/m$^2$, pulses of 5 ms and 10 ms reached complete desorption at absorbed energy densities of ca. 1.5 MJ/m$^2$. The desorption thresholds for these pulse durations were found experimentally at ca. 0.25, 0.5 and 0.75 MJ/m$^2$ by quantifying the desorbed deuterium as HD and $D_2$ by QMS. The remaining D in the laser spot was measured by NRA with a $^3$He beam showing a decrease of the remaining D with stronger laser heating until less than 1% of the initial D remained in the heated laser spots. As different extents of local delamination of ca. 20 µm large Be fragments were observed, these results had to be corrected by the missing Be amount, which was done by different compensation methods based on NRA, RBS and SEM. Slight changes in the microstructure and morphology of the layer, cracking of the layer and hill formation were observed in strong correlation with desorption. Hence, for such layers produced by HiPIMS they seem to be unavoidable during desorption. Nevertheless, in some cases of good layer adhesion, the delaminated area was only ca. 10% of the laser irradiated area even for the case of complete D desorption. These results encourage the development of LID on Be for the use in the tritium monitoring system in ITER. However, further studies on different layer thickness and D content and analysis of layers from the tokamak or stellarator are necessary to find the limitations of LID.

## Acknowledgments

The authors want to thank B. Göths for her help in preparation and polishing of the W substrates. This work was performed and funded under ITER contract IO/16/RFQ/13369/IDS and performed under EUROfusion WP PFC. This work has been carried out within the framework of the EUROfusion Consortium and has received funding from the Euratom research and training programme 2014–2018 under grant agreement No 633053. The views and opinions expressed herein do not necessarily reflect those of the European Commission or of the ITER Organization.

## References

[1] K. Heinola, et al., J. Nucl. Mater. 463 (2015) 961–965, https://doi.org/10.1016/j.jnucmat.2014.12.098.
[2] K. Schmid, Nucl. Fusion 55 (2015) 053015, , https://doi.org/10.1088/0029-5515/55/5/053015.
[3] G. De Temmerman, et al., Nucl. Mater. Eng. 12 (2017) 267–272, https://doi.org/10.1016/j.nme.2016.10.016.
[4] A. Huber, et al., Fusion Eng. Des. 86 (2011) 1336–1340, https://doi.org/10.1016/j.fusengdes.2011.01.090.
[5] S.E. Plansee, https://www.plansee.com/de/index.html (2018).
[6] P. Dinca, Surf. Coat. Technol. 321 (2017) 397–402, https://doi.org/10.1016/j.surfcoat.2017.04.074.
[7] V. Kh. Alimov, et al., Nucl. Instrum. Methods Phys. Res. B 234 (2005) 169–175, https://doi.org/10.1016/j.nimb.2005.01.009.
[8] M. Zlobinski, et al., Fuel Retention Diagnostic Setup (FREDIS) for desorption of gases from beryllium and tritium containing samples, Fusion Eng. Des. (2019), https://doi.org/10.1016/j.fusengdes.2019.02.035 in press, .
[9] M. Mayer, SIMNRA User's Guide, Max-Planck-Institut für Plasmaphysik, Garching, Germany, 1997 Report IPP 9/113 http://home.mpcdf.mpg.de/~mam/Report%20IPP%209-113.pdf.
[10] B. Spilker, Nucl. Fusion 56 (2016) 106014, , https://doi.org/10.1088/0029-5515/56/10/106014.
[11] D. Keroack, B. Terreault, J. Nucl. Mater. 212-215 (1994) 1443–1447, https://doi.org/10.1016/0022-3115(94)91066-9.
[12] J.H. Yu, et al., J. Nucl. Mater. 438 (2013) 1150–1154, https://doi.org/10.1016/j.jnucmat.2013.01.254.
[13] J.H. Yu, private communication.